

Recovery of metastable dense Bi synthesized by shock compression ^{EP}

Cite as: Appl. Phys. Lett. **114**, 120601 (2019); <https://doi.org/10.1063/1.5085678>

Submitted: 13 December 2018 . Accepted: 27 January 2019 . Published Online: 25 March 2019

M. G. Gorman ^{id}, A. L. Coleman, R. Briggs ^{id}, R. S. McWilliams, A. Hermann ^{id}, D. McGonegle, C. A. Bolme ^{id}, A. E. Gleason ^{id}, E. Galtier, H. J. Lee, E. Granados, E. E. McBride ^{id}, S. Rothman ^{id}, D. E. Fratanduono, R. F. Smith, G. W. Collins, J. H. Eggert, J. S. Wark, and M. I. McMahon ^{id}

COLLECTIONS

^{EP} This paper was selected as an Editor's Pick



View Online



Export Citation



CrossMark

ARTICLES YOU MAY BE INTERESTED IN

[Determination of bimolecular recombination constants in organic double-injection devices using impedance spectroscopy](#)

Applied Physics Letters **114**, 123301 (2019); <https://doi.org/10.1063/1.5066605>

[Setup for meV-resolution inelastic X-ray scattering measurements and X-ray diffraction at the Matter in Extreme Conditions endstation at the Linac Coherent Light Source](#)

Review of Scientific Instruments **89**, 10F104 (2018); <https://doi.org/10.1063/1.5039329>

[A critical review of recent progress on negative capacitance field-effect transistors](#)

Applied Physics Letters **114**, 090401 (2019); <https://doi.org/10.1063/1.5092684>

Applied Physics Reviews
Now accepting original research

2017 Journal
Impact Factor:
12.894

Recovery of metastable dense Bi synthesized by shock compression

Cite as: Appl. Phys. Lett. **114**, 120601 (2019); doi: [10.1063/1.5085678](https://doi.org/10.1063/1.5085678)

Submitted: 13 December 2018 · Accepted: 27 January 2019 ·

Published Online: 25 March 2019











View Online



Export Citation



CrossMark

M. G. Gorman,^{1,2,a)}  A. L. Coleman,¹ R. Briggs,^{1,2}  R. S. McWilliams,¹ A. Hermann,¹  D. McGonagle,³ C. A. Bolme,⁴  A. E. Gleason,⁵  E. Galtier,⁶ H. J. Lee,⁶ E. Granados,⁶ E. E. McBride,^{1,7}  S. Rothman,⁸  D. E. Fratanduono,² R. F. Smith,² G. W. Collins,⁹ J. H. Eggert,² J. S. Wark,³ and M. I. McMahon¹ 

AFFILIATIONS

¹SUPA, School of Physics & Astronomy, and Centre for Science at Extreme Conditions, The University of Edinburgh, Edinburgh EH9 3FD, United Kingdom

²Lawrence Livermore National Laboratory, 7000 East Avenue, Livermore, California 94500, USA

³Department of Physics, Clarendon Laboratory, Parks Road, University of Oxford, Oxford OX1 3PU, United Kingdom

⁴Shock and Detonation Physics, Los Alamos National Laboratory, P.O. Box 1663, Los Alamos, New Mexico 87545, USA

⁵Stanford Institute for Materials and Energy Sciences, SLAC National Accelerator Laboratory, Menlo Park, California 94025, USA

⁶Linac Coherent Light Source, SLAC National Accelerator Laboratory, Menlo Park, California 94025, USA

⁷SLAC National Accelerator Laboratory, Menlo Park, California 94025, USA

⁸Atomic Weapons Establishment, Aldermaston, Reading RG7 4PR, United Kingdom

⁹Departments of Mechanical Engineering, Physics and Astronomy, and Laboratory for Laser Energetics, University of Rochester, Rochester, New York 14627, USA

^{a)} Author to whom correspondence should be addressed: gorman1@llnl.gov

ABSTRACT

X-ray free electron laser (XFEL) sources have revolutionized our capability to study ultrafast material behavior. Using an XFEL, we revisit the structural dynamics of shock compressed bismuth, resolving the transition sequence on shock release in unprecedented details. Unlike previous studies that found the phase-transition sequence on shock release to largely adhere to the equilibrium phase diagram (i.e., Bi-V \rightarrow Bi-III \rightarrow Bi-II \rightarrow Bi-I), our results clearly reveal previously unseen, non-equilibrium behavior at these conditions. On pressure release from the Bi-V phase at 5 GPa, the Bi-III phase is not formed but rather a new metastable form of Bi. This new phase transforms into the Bi-II phase which in turn transforms into a phase of Bi which is not observed on compression. We determine this phase to be isostructural with β -Sn and recover it to ambient pressure where it exists for 20 ns before transforming back to the Bi-I phase. The structural relationship between the tetragonal β -Sn phase and the Bi-II phase (from which it forms) is discussed. Our results show the effect that rapid compression rates can have on the phase selection in a transforming material and show great promise for recovering high-pressure polymorphs with novel material properties in the future.

<https://doi.org/10.1063/1.5085678>

Bismuth is an archetypal semi-metallic phase-transforming material, long studied to elucidate the response of multiphase metals to high stress.^{1–5} Up to 8 GPa and 600 K, static compression studies have shown Bi to exhibit a rich structural complexity, existing in five different solid phases,^{6–9} most notably the tetragonal Bi-III phase (stable between 2.7 and 7.7 GPa at 300 K) which has an incommensurate host-guest structure.⁸ While the phase behavior of Bi has also been studied extensively under shock compression,^{10–16} the structural response of Bi to rapid pressure loading was only recently revealed by using *in situ* X-ray diffraction from an X-ray free electron laser

(XFEL) and was found to deviate significantly from the transformation behavior observed under static compression.¹⁷ While the dynamic experiments observed the Bi-I (rhombohedral) \rightarrow Bi-II (monoclinic) transition on compression at conditions that are in good agreement with previous static studies, the incommensurate Bi-III phase was not observed, but rather a new metastable phase of Bi termed Bi-M. Above 4 GPa, only the Bi-V (body-centered cubic) phase was observed. These results show that the assumption of equilibrium behavior under shock compression, which has often been made to help interpret data from traditional shock experiments, can be invalid for complex materials.

Phase transformations have previously been inferred in Bi on shock release,^{18,19} but the interpretation of these results has been complicated by multiple waves traveling through the released Bi sample. Hu *et al.* performed X-ray structural studies of Bi on shock release and reported the transition sequence to be in accordance with the equilibrium phase diagram (i.e., Bi-V \rightarrow Bi-III \rightarrow Bi-II \rightarrow Bi-I).²⁰ However, the low-fluence X-ray probe used in these experiments led to only tentative phase assignments to the diffraction data and, as a result, the structural behavior of Bi on shock release is still not definitively known. This key experimental challenge can now be overcome with the use of fourth generation XFEL light sources which can produce femtosecond pulses of X-ray radiation that are 9 orders of magnitude brighter than 3rd generation synchrotron sources.

Here, we have revisited the structural dynamics of Bi on shock release using high-quality *in situ* diffraction from an XFEL and found the transition sequence of Bi on shock release from 5 GPa to differ from the equilibrium picture reported recently.²⁰ Instead, we found the transition sequence to be similar to, but not the reverse of, the sequence recently observed on shock compression.¹⁷ While the Bi-V, newly observed Bi-M and Bi-II phases are all observed on shock release, the Bi-II \rightarrow Bi-I back transformation is not, but rather a transition to another metastable phase which we determine to be isostructural with β -Sn and closely related to the Bi-II structure. This phase is observed to be recoverable to ambient pressure and exist for up to 20 ns after shock release before finally transforming back to the Bi-I phase. Our results clarify the complex structural dynamics of Bi on shock release, while the quenching of a high-pressure phase to ambient for tens of nanoseconds shows great promise for the synthesis of high-density novel materials in the future.

Experiments were performed at the Matter in Extreme Conditions (MEC) end station of the Linac Coherent Light Source (LCLS) at the Stanford National Accelerator Laboratory.²¹ We employed the standard configuration experimental setup at MEC as shown in Fig. 1. A Nd-glass optical laser (527 nm, 20 ns quasi-flat-topped pulse duration) was used to launch an ablation-driven shock wave through the samples, which consisted of 8 μm of Bi sputter-deposited onto a 50 μm thick polyimide ablator. The LCLS provided quasi-monochromatic ($\Delta E/E = 0.5\%$) 10.0 keV X-ray pulses of 80 fs duration and with $\sim 10^{12}$ photons per pulse. The X-ray beam was focused onto $50 \times 50 \mu\text{m}^2$ and then centered on the $\sim 500 \mu\text{m}$ diameter focal-spot of the drive lasers, which, in turn, was centered on the target. Diffraction patterns were collected on an array of 5 CSPAD area detectors arranged in a Debye-Scherrer geometry behind the sample (Fig. 1). The sample-to-detector distances and tilts of each detector were determined using diffraction patterns collected from CeO₂ and LaB₆ standards. The 2D images from the 5 detectors were then integrated and combined to provide 1D profiles covering a 2θ range of $\sim 20^\circ$ – 110° .

The target free surface velocity history was recorded using the VISAR (velocity interferometry system for any reflector) diagnostic which was used to determine the peak sample pressure, the time of shock breakout, and the planarity of drive. The Bi samples were initially shock compressed to a peak pressure of ~ 5 GPa and then, by increasing the delay of the XFEL probe beam relative to the optical laser drive for subsequent shots, diffraction was collected on identically driven targets as the shock wave travelled through the Bi sample and after the shock wave broke out at the rear surface. To complement our

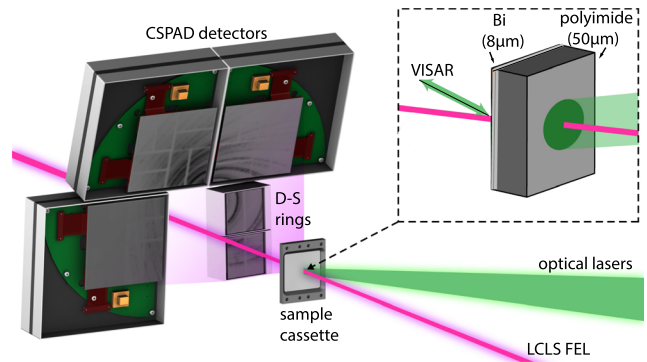


FIG. 1. Experimental setup and 2D diffraction data: (a) Cornell Stanford Pixel Array Detectors (CS PADS) are arranged in transmission Debye-Scherrer geometry in the MEC vacuum chamber. Dual drive beams are incident on the target at an angle of 15° and the XFEL beam probes the target 30° from the target normal. The VISAR laser probes normal to the rear surface of the target. The target design consisted of 8 μm of Bi which was sputter deposited onto a 50 μm polyimide ablator. Adapted from Ref. 17. Reprinted with permission from M. G. Gorman, A. L. Coleman, R. Briggs, R. S. McWilliams, D. McGonegle, C. A. Bolme, A. E. Gleason, E. Galtier, H. J. Lee, E. Granados *et al.*, *Sci. Rep.* **8**, 16927 (2018). Copyright 2018 Author(s), licensed under a Creative Commons Attribution 4.0 License.

experiments, density functional theory (DFT) total energy calculations were performed using a plane wave basis set in conjunction with the projector-augmented wave method as implemented in the Vienna Ab Initio Simulation Package (VASP) package.^{22,23} We considered the Bi $5d^{10}6s^26p^3$ electrons in the valence space and included spin-orbit coupling (supplementary material). Electron-electron interactions were approximated using the Perdew-Burke-Ernzerhof (PBE) exchange-correlation functional.²⁴ The incommensurate Bi-III phase was modeled using a 32-atom approximant with $P4/ncc$ symmetry.

Diffraction from the unshocked sample shows that, as expected, Bi initially existed in the ambient Bi-I phase [Fig. 2(i-a)]. At $t = -2$ ns, i.e., 2 ns before the shock wave broke out at the rear surface, and at a peak pressure of 5 GPa, diffraction from the Bi-V and compressed Bi-I phases was observed, in addition to diffraction from uncompressed Bi-I ahead of the shock wave, indicating a direct Bi-I \rightarrow Bi-V transformation [Fig. 2(i-b)]. The diffraction from the compressed Bi-I phase originates from the splitting of the shock front in the sample at the Bi-I \rightarrow Bi-V transformation point as a result of $\sim 10\%$ volume collapse at the transition.¹⁴ This splitting was clearly evident as a two-wave profile in the measured VISAR trace (supplementary material).

After the shock wave broke out at the rear surface at $t = 0$, strong release waves entered the sample, which introduced significant pressure gradients in it, with pressures ranging from the peak pressure to zero. As a result, diffraction data collected after $t = 0$ showed diffraction peaks from multiple phases originating from the different regions of the sample at different pressure conditions. At $t = +3$ ns, i.e., 3 ns after shock breakout, the diffraction showed that some of the sample remained in the Bi-V phase, but other regions had transformed into the metastable Bi-M phase, as observed previously,¹⁷ and the Bi-II phase [Fig. 2(i-c)]. Later in time (at $t = +9$ ns), no diffraction from the Bi-V phase was observed, showing that all of the sample had released from peak pressure, but diffraction from the Bi-M and Bi-II phases was still present [Fig. 2(i-d)]. However, at $t = +17$ ns, the diffraction pattern simplified greatly, as diffraction peaks from the Bi-M and Bi-II

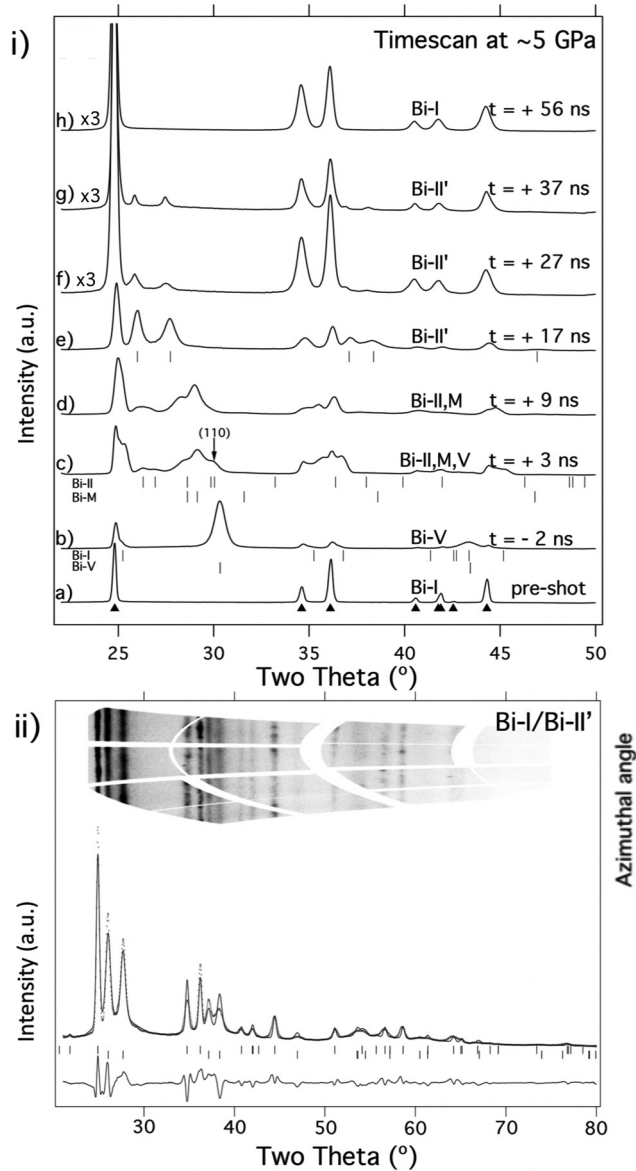


FIG. 2. (i) Waterfall plot of X-ray diffraction data collected from identically driven Bi samples with increasing XFEL delay time ($\lambda = 1.409$ Å). The observed phases are labelled and the expected peaks from them are shown by tick marks beneath the profiles. The diffraction peaks from the ambient Bi-I phase are shown as black triangles. The (110) reflection of the Bi-V phase in profile (c) is marked with an arrow. (ii) A two phase (40%:60%) released Bi-I : Bi-II' Rietveld fit to the diffraction profile obtained at $t = +17$ ns with de-warped raw diffraction data overlaid. The calculated positions of the best-fitting Bi-I and Bi-II' unit cells are shown in upper and lower tick marks beneath the profile.

phases disappeared and were replaced by 11 new Bragg reflections. Analysis of their positions and intensities reveals that they could all be explained as coming from a structure identical to that of tetragonal β -Sn with space group $I4_1/amd$ and refined lattice parameters $a = 6.276$ Å and $c = 3.336$ Å with the density determined to be 7%

greater than ambient Bi-I [Figs. 2(i-e) and 2(ii)]. At $t = +27$ ns [Fig. 2(i-f)], diffraction peaks from this phase persisted, although they were weaker, and the determined lattice parameters had increased to $a = 6.315$ Å and $c = 3.370$ Å with the density 5% greater than ambient Bi-I. These values did not change further for data collected at $t = +37$ ns [Fig. 2(i-g)], suggesting that the β -Sn phase was at ambient pressure at both $t = +27$ ns and $+37$ ns. At $t = +56$ ns, diffraction peaks from the β -Sn phase were no longer present and only the ambient pressure Bi-I phase was observed [Fig. 2(i-h)].

As the β -Sn phase of Bi is observed late in time on release and in the absence of any other high-pressure phases, it is reasonable to assume that it is formed via a transition from the phase present in the sample immediately before its emergence, that is, the monoclinic Bi-II phase. The β -Sn phase has been reported previously in both large volume press²⁵ and diamond anvil cell²⁶ studies, where it has been suggested that it is the high-pressure high-temperature Bi-II' phase and that it is stable only between 1.8–2.0 GPa and 450–470 K. It has never been observed before under dynamic compression. A Rietveld refinement fit to the $t = +17$ ns profile using a two phase Bi-I : Bi-II' model is shown in Fig. 2(ii) and is excellent, accounting for both the positions and intensities of the observed diffraction peaks. The inset to Fig. 2(ii) shows that the diffraction peaks from Bi-I after release are markedly different from the spotty, textured diffraction peaks of the Bi-starting material (supplementary material), demonstrating that significant microstructural rearrangement has occurred through numerous phase transformations on shock compression and release.

In order to elucidate the nature of the Bi-II \rightarrow Bi-II' transition, we have made extensive DFT studies of Bi up to 10 GPa. These reveal that a transformation between the Bi-II' and Bi-II phases should not be unexpected, as the two phases are energetically within 5 meV/atom of each other up to about 7 GPa (Fig. 3). The atomic volume of the ambient pressure Bi-II' phase observed in our experiments ($V = 33.6$ Å³) agrees very well with the calculated volume from our DFT calculations at 0 K ($V = 34.3$ Å³) (supplementary material). The observation of the Bi-II' phase at ambient pressure for ~ 20 ns, despite the high sample temperature, is surprising and suggests a kinetically inhibited transition between the Bi-II' and Bi-I structures. Hu *et al.* observed a sluggish transformation to Bi-I from a high-pressure phase which they reported to be Bi-II and cited the reconstructive nature of the Bi-II \rightarrow Bi-I transition as a possible explanation.²⁰ Our results show that the phase actually observed in the study of Hu *et al.* was likely the Bi-II' phase and the data quality in that study made it impossible to distinguish it from Bi-II. As the $I4_1/amd$ and $R\bar{3}m$ space groups of Bi-II' and Bi-I, respectively, are not group-subgroup related, the transformation from Bi-II' to Bi-I, like the transition from Bi-II \rightarrow Bi-I transition, would involve significant atomic rearrangement which could explain the kinetic hindrance observed in our experiments. Indeed, from multi-phase Rietveld analysis of the diffraction data, the measured phase fraction of Bi-II' at $t = 17$ ns [Fig. 2(i-e)] is 60%, which decreased to only 4% at $t = 27$ ns, 2% at $t = 37$ ns, and 0% at $t = 56$ ns. The rate of transformation from Bi-II' back to Bi-I is approximately an order of magnitude slower than models from classical nucleation theory, which shows that after a certain incubation time, the new phase is nucleated throughout the sample at the speed of sound.²⁷

The observation of the Bi-II' phase forming from Bi-II on shock release allows for examination of the phase transformation

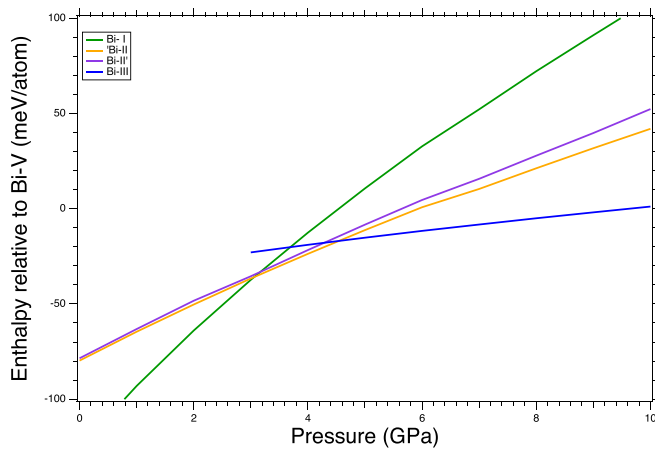


FIG. 3. The results of DFT calculations showing the enthalpies of the equilibrium phases of Bi relative to the Bi-V phase as a function of pressure and at zero temperature. The Bi-II' phase (purple line) is energetically similar to the Bi-II phase (orange line) up to 7 GPa.

mechanism. The monoclinic Bi-II structure, unique to Bi, has long been described as a heavily distorted primitive cubic lattice.²⁸ However, the structures of Bi-II and Bi-II' are group-subgroup related, such that the tetragonal Bi-II' structure can be equally well described by a modified Bi-II structure. The Bi-II' structure with space group $I4_1/amd$ at 2.0 GPa with $a = 6.222 \text{ \AA}$ and $c = 3.320 \text{ \AA}$ and atoms on the 4(a) Wyckoff site $(0, 0, 0)$ can be equally well described in monoclinic space group $C2/m$ with $a' = 7.052 \text{ \AA}$, $b' = 6.222 \text{ \AA}$, $c' = 3.320 \text{ \AA}$, $\beta' = 118.08^\circ$ with atoms on the 4(i) site at $(\frac{1}{4}, 0, \frac{1}{8})$ [Fig. 4(i)]. The actual Bi-II structure at 2.0 GPa has $a = 6.663 \text{ \AA}$, $b = 6.181 \text{ \AA}$, $c = 3.312 \text{ \AA}$, $\beta = 110.93^\circ$, and atoms on the 4(i) sites at $(0.249, 0, 0.137)$.⁵ The principal structural changes during the Bi-II \rightarrow Bi-II' transformation are then an 8° shear of the β angle and an $\sim 5\%$ expansion of the a -axis, but with little relative movement of the atoms. We investigated the energetics of this deformation [Fig. 4(ii)] and found that the Bi-II' structure (transition coordinate = 0) is a local energy minimum relative to the equilibrium Bi-II structure (transition coordinate = 1) below 4 GPa. The rapid decompression rates (10^9 GPa/s) and shear forces experienced by the Bi sample in our experiments may play a crucial role in accessing this local energy minimum.

The ability to recover Bi-II' to ambient pressure, the density of which is $\sim 5\%$ greater than that of Bi-I, has implications for controlling metal damage under dynamic strain such as in armors: if the release from high pressure conditions can be made more gradual, e.g., by kinetic hindrance and transient persistence of high pressure phases, the degree of damage could be reduced, e.g., by controlling the magnitudes of tensile stress and preventing spallation. Better characterization of the mechanisms of the structural forward- and back-transformations can inform new approaches to producing other novel phases of matter at ambient conditions and lead to improved strategies for damage reduction in materials under dynamic loads. Recovering Bi-II' also has clear implications for the field of material synthesis where the recovery of high-pressure solid phases with novel physical and electronic properties is a major goal. We demonstrate that the rapid decompression rates accessed using shock waves may be key to stabilizing high-pressure phases of materials and prove fruitful for synthesizing

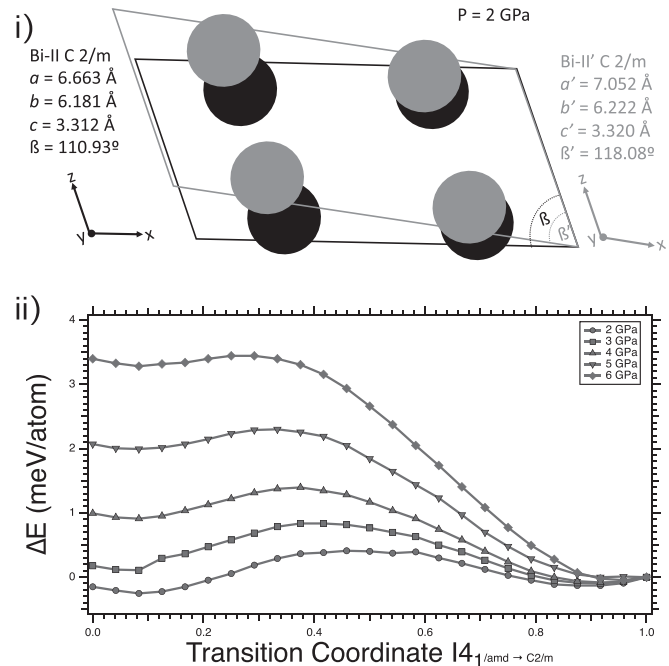


FIG. 4. (i) The structural relationship between Bi-II (black) and Bi-II' (grey) as viewed along the b axis. The body-centered tetragonal β -Sn structure of Bi-II' can be represented in the $C 2/m$ setting. The main structural changes in the Bi-II \rightarrow β -Sn transformation are an 8° shear of the β angle and an $\sim 5\%$ expansion of the a lattice parameter. (ii) DFT calculations of the energetics of the Bi-II-Bi-II' transition. Bi-II' is found to be a local energy minimum below 4 GPa.

novel phases of technologically important materials such as the metastable ST12 phase of Si, which is predicted to be superconducting.^{29,30}

In summary, we have definitively mapped out the structural dynamics of bismuth on shock release from 5 GPa. Contrary to previous studies which reported the transition sequence to be consistent with the static phase diagram, our data reveal a marked departure from equilibrium behavior at these conditions with the absence of the Bi-III phase and the recovery of a high-pressure metastable phase not observed on shock compression, which we determine to be isostructural with β -Sn. The high-quality X-ray diffraction data achievable at XFEL sources have revolutionized our ability to resolve the ultrafast structural response of materials to shock compression. These sources will be essential in our effort towards a better understanding of the effect of compression rate on the kinetics of phase transformations in complex materials.

See [supplementary material](#) for discussion on the sample microstructure, wave profiles, and DFT calculations.

British Crown Owned Copyright 2018/AWE. M.I.M and J.S.W would like to acknowledge support from EPSRC under Grant Nos. EP/J017256/1 and EP/J017051/1. D.M. was supported by LLNS under Contract No. B595954. The work by J.H.E., D.E.F., and R.F.S. was performed under the auspices of the U.S. Department of Energy by Lawrence Livermore National Laboratory under Contract No. DE-AC52-07NA27344. C.A.B. would like to acknowledge support from

Science Campaign 2 at Los Alamos National Laboratory, which is operated for the National Nuclear Security Administration of the U.S. Department of Energy under Contract No. DE-AC52-06NA25396. The use of the Linac Coherent Light Source (LCLS), SLAC National Accelerator Laboratory, was supported by the U.S. Department of Energy, Office of Science, Office of Basic Energy Sciences under Contract No. DE-AC02-76SF00515. The MEC instrument was supported by the U.S. Department of Energy, Office of Science, Office of Fusion Energy Sciences under Contract No. SF00515. We would like to thank Carol A. Davis and Paul Mirkirimi of LLNL for their help in preparing the Bi targets.

REFERENCES

- ¹J. W. Klement, A. Jayaraman, and G. C. Kennedy, *Phys. Rev.* **131**, 632 (1963).
- ²D. Balla and N. B. Brandt, *Sov. Phys. JETP* **20**, 1111 (1965).
- ³A. Yoneda and S. Endo, *J. Appl. Phys.* **51**, 3216 (1980).
- ⁴H.-Y. Chen, S.-K. Xiang, X.-Z. Yan, L.-R. Zheng, Y. Zhang, S.-G. Liu, and Y. Bi, *Chin. Phys. B* **25**, 108103 (2016).
- ⁵O. Degtyareva, M. I. McMahon, and R. J. Nelmes, *High Pressure Res.* **24**, 319 (2004).
- ⁶L. G. Akselrud, M. Hanfland, and U. Schwarz, *Z. Kristallogr. - New Cryst. Struct.* **218**, 415 (2003).
- ⁷R. M. Brugger, R. B. Bennion, and T. G. Worlton, *Phys. Lett. A* **24**, 714 (1967).
- ⁸M. I. McMahon, O. Degtyareva, and R. J. Nelmes, *Phys. Rev. Lett.* **85**, 4896 (2000).
- ⁹W. Chaimayo, L. F. Lundegaard, I. Loa, G. W. Stinton, A. R. Lennie, and M. I. McMahon, *High Pressure Res.* **32**, 442 (2012).
- ¹⁰R. E. Duff and F. S. Minshall, *Phys. Rev.* **108**, 1207 (1957).
- ¹¹D. S. Hughes, L. E. Gourley, and M. F. Gourley, *J. Appl. Phys.* **32**, 624 (1961).
- ¹²D. B. Larson, *J. Appl. Phys.* **38**, 1541 (1967).
- ¹³J. R. Asay, *J. Appl. Phys.* **45**, 4441 (1974).
- ¹⁴J. P. Romain, *J. Appl. Phys.* **45**, 135 (1974).
- ¹⁵J. L. Pélissier and D. Partouche-Sebban, *Phys. B: Condens. Matter* **364**, 14 (2005).
- ¹⁶Y. Tan, Y. Yu, C. Dai, K. Jin, Q. Wang, J. Hu, and H. Tan, *J. Appl. Phys.* **113**, 093509 (2013).
- ¹⁷M. G. Gorman, A. L. Coleman, R. Briggs, R. S. McWilliams, D. McGonegle, C. A. Bolme, A. E. Gleason, E. Galtier, H. J. Lee, E. Granados *et al.*, *Sci. Rep.* **8**, 16927 (2018).
- ¹⁸J. R. Asay, *J. Appl. Phys.* **48**, 2832 (1977).
- ¹⁹Z. Rosenberg, *J. Appl. Phys.* **56**, 3328 (1984).
- ²⁰J. Hu, K. Ichiyanagi, T. Doki, A. Goto, T. Eda, K. Norimatsu, S. Harada, D. Horiuchi, Y. Kabasawa, S. Hayashi *et al.*, *Appl. Phys. Lett.* **103**, 161904 (2013).
- ²¹S. Moeller, J. Arthur, A. Brachmann, R. Coffee, F. J. Decker, Y. Ding, D. Dowell, S. Edstrom, P. Emma, Y. Feng *et al.*, *Nucl. Instrum. Methods Phys. Res., Sect. A* **635**, S6 (2011).
- ²²G. Kresse and J. Furthmüller, *Phys. Rev. B* **54**, 11169 (1996).
- ²³G. Kresse and D. Joubert, *Phys. Rev. B* **59**, 1758 (1999).
- ²⁴J. P. Perdew, K. Burke, and M. Ernzerhof, *Phys. Rev. Lett.* **77**, 3865 (1996).
- ²⁵E. Principi, M. Minicucci, A. Di Cicco, A. Trapananti, S. De Panfilis, and R. Poloni, *Phys. Rev. B* **74**, 064101 (2006).
- ²⁶C. Lin, J. S. Smith, S. V. Sinogeikin, Y. Kono, C. Park, C. Kenney-Benson, and G. Shen, *Nat. Commun.* **8**, 14260 (2017).
- ²⁷M. D. Knudson and Y. M. Gupta, *J. Appl. Phys.* **91**, 9561 (2002).
- ²⁸H. Katzke and P. Tolédano, *Phys. Rev. B* **77**, 024109 (2008).
- ²⁹B. D. Malone, J. D. Sau, and M. L. Cohen, *Phys. Rev. B* **78**, 035210 (2008).
- ³⁰L. Rapp, B. Haberl, C. J. Pickard, J. E. Bradby, E. G. Gamaly, J. S. Williams, and A. V. Rode, *Nat. Commun.* **6**, 7555 (2015).